Ionization of hydrogen atoms in attosecond pulse trains and strong infrared laser pulses

Sen Cui,[1] Pei-Lun He,[1] and Feng He[1,2,*]

[1]*Key Laboratory for Laser Plasmas (Ministry of Education) and Department of Physics and Astronomy, Shanghai Jiao Tong University, Shanghai 200240, China*

[2]*Collaborative Innovation Center of IFSA (CICIFSA), Shanghai Jiao Tong University, Shanghai 200240, China*

(Received 2 August 2016; published 1 November 2016)

Ionization of a hydrogen atom exposed to an attosecond pulse train and a few-cycle middle infrared (MIR) pulse is calculated with the strong field approximation. The ionization events initiated by two attosecond pulses in the train are streaked in the presence of a weak MIR pulse, making the two ionization events overlap or separate in momentum representation. By changing the weak MIR pulse intensity, the interference structure in the photoelectron momentum distribution can be precisely tailored. When the MIR field is strong enough to produce substantial ionization, the overlapped attosecond pulse train and MIR field trigger the XUV-phase-dependent photoelectron angular distribution. Either the interference pattern or the angular distribution can be used to extract the carrier envelope phase of attosecond pulses, which makes it possible to visualize the sub-XUV-cycle dynamics.

DOI: 10.1103/PhysRevA.94.053401

I. INTRODUCTION

The advent of ultrashort laser technologies provides a tool to observe and manipulate ultrafast dynamics of atoms and molecules [1,2]. Ionization, as the most fundamental process of atoms in strong laser fields, has been extensively studied in past decades. Ionization can be divided into multiphoton and tunneling scenarios [3–6], depending on the Keldysh parameter [7] $\gamma = \sqrt{I_p/2U_p}$, where I_p is the ionization potential and U_p is the ponderomotive energy where $U_p = I/4\omega^2$ with I and ω being the laser intensity and frequency in atomic units. When $\gamma \gg 1$, the electron absorbs one or several photons, and leaves its parent ion by taking the excess energy $n\hbar\omega - I_p$ where n is the number of the absorbed photons. In contrast, when $\gamma \ll 1$, the electron sees a quasistatic electric field and tunnels out the laser-distorted Coulomb potential. The freed electron carries the momentum equating to the opposite value of the laser vector potential at the tunneling moment if the Coulomb field action can be neglected. The tunneling electron may rescatter with its parent core accompanied with high harmonic generation [8,9], double ionization [10–12], electron excitation [13], and so on. The freed electron propagation can be manipulated by several strategies, for example, using an elliptically polarized laser pulse to suppress the electron-ion rescattering [14,15] and using multiple pulses to control the ionization and rescattering timing [16]. The rescattered electron wave packet can be used to image atomic or molecular structures [17–21].

With the help of isolated attosecond pulses, people are able to deeply look into the ionization process with unprecedented time resolutions. By combing the single attosecond pulse with a few-cycle phase-stabilized infrared pulse, one may observe the light-induced electron tunneling in real time [22,23]. Photoionization probabilities and photoabsorption can be controlled by tuning the delay between the attosecond pulse and the infrared pulse [24–26], in which scenarios the MIR laser field shifts the energy levels and induces destructive or constructive transition between different electronic states. In the combined XUV and MIR fields, the XUV-freed electron is streaked by the time-delayed MIR pulse, and the streaked electron spectrogram can be used to reconstruct the XUV pulse duration and spectra phases [27]. In contrast, the infrared laser waveform can be extracted from the streaked electron momentum spectra [28,29].

Experimentally, the attosecond pulse train [30] is used more widely than the isolated attosecond pulse because the former can be produced more easily. A train of attosecond pulses synchronized with an infrared laser pulse may contribute a delay-dependent photoionization probability [31–33]. The dissociative ionization of small molecules such as H_2 can be probed by the attosecond pulse train in the presence of a near-infrared field [34]. The attosecond pulse train may produce the replicas of the nuclear wave packet during the molecular ionization; however, the summation of all nuclear wave packets is prone to be added incoherently because of the entanglement between the freed electron and its parent molecular ion [35].

Using an isolated XUV pulse plus a weak infrared laser pulse, the XUV-induced photoelectron will be streaked by the infrared field. Depending on the XUV pulse duration, one may obtain the streaked photoelectron spectrogram or side bands [36–40]. For an attosecond pulse train and a weak infrared pulse, one may expect more complex photoelectron momentum distribution (PMD) because the ionization events induced by different attosecond pulses in the train may interfere with each other. This interference structure can be manipulated by the infrared field. In this paper, we use the strong field approximation (SFA) to calculate the PMD of a hydrogen atom in an attosecond pulse train and a few-cycle MIR pulse. We use a MIR field because it may streak the photoelectron momentum in a larger range than the infrared laser with the same intensity does. We vary the MIR intensity in a quite large range, and the PMD presents very different structures, from which the relative phase between different attosecond pulses can be retrieved. The rest of the paper is organized as following. In Sec. II, we introduce the theoretical model used for calculating the photoionization. In Sec. III, the PMDs obtained with different MIR

*fhe@sjtu.edu.cn

intensities are presented. The paper ends with a conclusion in Sec. IV.

II. THEORETICAL MODELS

We use the SFA [7,41–43] to calculate the PMD. In our process, the high-energetic XUV photon kicks off the electron in a hydrogen atom and the freed electron escapes quickly. Thus the Coulomb potential can be neglected and the SFA is justified. The electron transition amplitude is described as (atomic units are used unless stated otherwise)

$$M(p) = -i \int_{t_0}^{t} dt' \langle \boldsymbol{p} + \boldsymbol{A}(t') | \boldsymbol{r} \cdot \boldsymbol{E}(t') | \Psi_0 \rangle e^{iS_p(t') + iI_p(t'-t_0)} \tag{1}$$

with the Volkov phase $S_p(t') = \frac{1}{2}\int_{t_0}^{t'} dt''[\boldsymbol{p} + \boldsymbol{A}(t'')]^2$ and the electric field $\boldsymbol{E}(t) = -\frac{d\boldsymbol{A}(t)}{dt}$, Ψ_0 being the hydrogen atom ground state and t_0 being the starting time of the laser field. The ionization potential of a hydrogen atom is $I_p = 0.5$ a.u. The laser vector potential **A** comprises a MIR field and two XUV pulses spaced by half a MIR period, which are written as

$$A_x(t) = A_{x,xuv1}(t) + A_{x,xuv2}(t) + A_{x,\mathrm{mir}}(t), \tag{2}$$

$$A_y(t) = A_{y,xuv1}(t) + A_{y,xuv2}(t) + A_{y,\mathrm{mir}}(t), \tag{3}$$

where

$$A_{x,xuv1}(t) = A_{0,xuv} \sin\left[\omega_{xuv}\left(t + \frac{T_{\mathrm{mir}}}{4}\right)\right] \cos^2\left[\frac{\pi\left(t + \frac{T_{\mathrm{mir}}}{4}\right)}{\tau_{xuv}}\right], \quad -\tau_{xuv}/2 - T_{\mathrm{mir}}/4 < t < \tau_{xuv}/2 - T_{\mathrm{mir}}/4 \tag{4}$$

$$A_{x,xuv2}(t) = A_{0,xuv} \sin\left[\omega_{xuv}\left(t - \frac{T_{\mathrm{mir}}}{4}\right) + \phi\right] \cos^2\left[\frac{\pi\left(t - \frac{T_{\mathrm{mir}}}{4}\right)}{\tau_{xuv}}\right], \quad -\tau_{xuv}/2 + T_{\mathrm{mir}}/4 < t < \tau_{xuv}/2 + T_{\mathrm{mir}}/4 \tag{5}$$

$$A_{x,\mathrm{mir}}(t) = A_{0,\mathrm{mir}} \sin(\omega_{\mathrm{mir}} t) \cos^2\left[\frac{\pi t}{\tau_{\mathrm{mir}}}\right], \quad -\tau_{\mathrm{mir}}/2 < t < \tau_{\mathrm{mir}}/2 \tag{6}$$

$$A_{y,xuv1}(t) = A_{0,xuv} \cos\left[\omega_{xuv}\left(t + \frac{T_{\mathrm{mir}}}{4}\right)\right] \cos^2\left[\frac{\pi(t + \frac{T_{\mathrm{mir}}}{4})}{\tau_{xuv}}\right], \quad -\tau_{xuv}/2 - T_{\mathrm{mir}}/4 < t < \tau_{xuv}/2 - T_{\mathrm{mir}}/4 \tag{7}$$

$$A_{y,xuv2}(t) = A_{0,xuv} \cos\left[\omega_{xuv}\left(t - \frac{T_{\mathrm{mir}}}{4}\right) + \phi\right] \cos^2\left[\frac{\pi(t - \frac{T_{\mathrm{mir}}}{4})}{\tau_{xuv}}\right], \quad -\tau_{xuv}/2 + T_{\mathrm{mir}}/4 < t < \tau_{xuv}/2 + T_{\mathrm{mir}}/4 \tag{8}$$

$$A_{y,\mathrm{mir}}(t) = A_{0,\mathrm{mir}} \cos(\omega_{\mathrm{mir}} t) \cos^2\left[\frac{\pi t}{\tau_{\mathrm{mir}}}\right], \quad -\tau_{\mathrm{mir}}/2 < t < \tau_{\mathrm{mir}}/2, \tag{9}$$

where the XUV pulse durations τ_{xuv} and τ_{mir} have three and four cycles, respectively. The XUV and MIR wavelengths are 40 and 1600 nm, respectively. The carrier envelope phases (CEPs) of the first XUV and MIR field are both fixed at 0, while the second XUV has a variable CEP. The XUV and MIR intensities are modulated for different purposes. When linearly polarized pulses are used, we simply omit the component of $A_y(t)$. Figures 1(a) and 1(b) plot the linearly and circularly polarized XUV pulse train plus the MIR field, respectively. The x and y components of the circularly polarized field are projected onto the bottom and back planes in Fig. 1(b).

III. SIMULATION RESULTS

When the atom is exposed to the attosecond pulse train, the electron absorbs a high-energetic XUV photon and escapes with the momentum $p = \pm\sqrt{2(\omega - I_p)}$. For attosecond pulses spaced by half a T_{mir} and the MIR pulse not introduced, the photoelectron momenta show a series of peaks corresponding to energy peaks spaced by $2\omega_{\mathrm{mir}}$, as shown in Figs. 1(c) and 1(d). In the presence of another weak MIR field, the photoelectron will be streaked and acquire a momentum shift equating to the opposite value of the MIR vector potential at the releasing moment. The two ionization events triggered by XUV1 and XUV2 see opposite laser vector potentials; thus they will be shifted negatively and positively along the x axis. Such streaks separate parts of the momenta initiated by XUV1 and XUV2 and thus clear up the interference peaks; meanwhile, other parts of the momenta are packed together by forming concentric rings in the middle, as shown in Figs. 1(e) and 1(f). If the laser vector potential $|A_x| > \sqrt{2(\omega_{xuv} - I_p)}$, one may expect that the two ionization events triggered by two XUV pulses will not meet in the momentum representation; thus no any interference structure but only two separated circles are obtained. The PMD obtained with more MIR intensities can be observed in the movies in the Supplemental Material [44].

For the linear and circular streaking, the most distinct difference is that the up-down symmetry in Fig. 1(e) is broken in Fig. 1(f). To understand the mechanism governed for such symmetry broken, the line out at $p_x = 0$ in Fig. 1(f) is plotted in Fig. 2(a). The erratic curve becomes regular if the origin of the coordinate is shifted to the center of the concentric rings of the interference pattern in Fig. 1(f), i.e., making a transformation $p'_y = p_y - 0.4$. The p'_y spectrum corresponds to a series of energy peaks spaced by $2\omega_{\mathrm{mir}}$, as shown in Fig. 2(b). The black and blue lines correspond to negative and positive p'_y, respectively. Such a momentum transformation along the y axis can be understood by looking into the phase in Eq. (1). The two ionization events initiated by the two XUV pulses

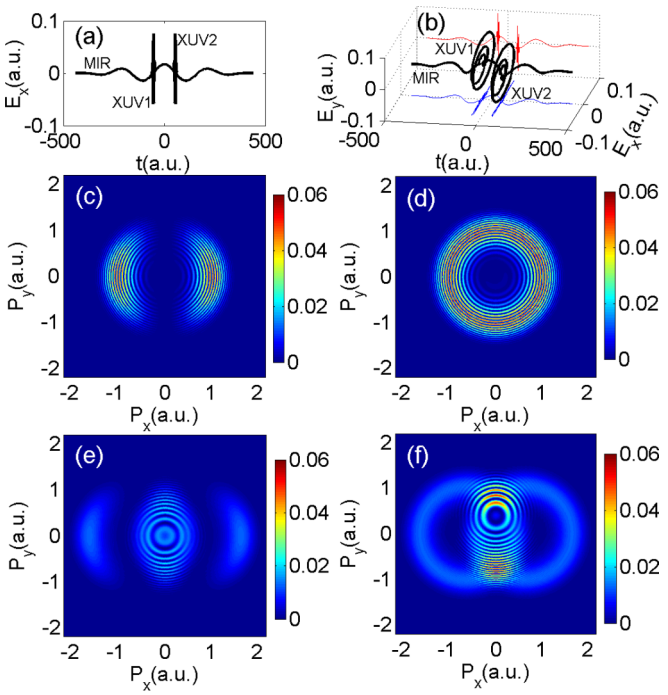

FIG. 1. (a) The combined linearly polarized XUV pulse train and linearly polarized MIR field. (b) The combined circularly polarized XUV pulse train and circularly polarized MIR field. The $E_x(t)$ and $E_y(t)$ are projected in the bottom and back planes. In panels (a) and (b), the MIR intensities are 1.2×10^{13} and 2.4×10^{13} W/cm^2, respectively; the XUV pulse train intensities are 2×10^{14} and 4×10^{14} W/cm^2, respectively. Panels (c) and (d): The PMDs triggered by the XUV pulse trains in panels (a) and (b), respectively. The MIR field is not introduced for these two panels. Panels (e) and (f): The PMDs produced by the combined laser fields in panels (a) and (b), respectively. The XUV wavelength is 40 nm, and the MIR wavelength is 1600 nm. $\phi = 0$.

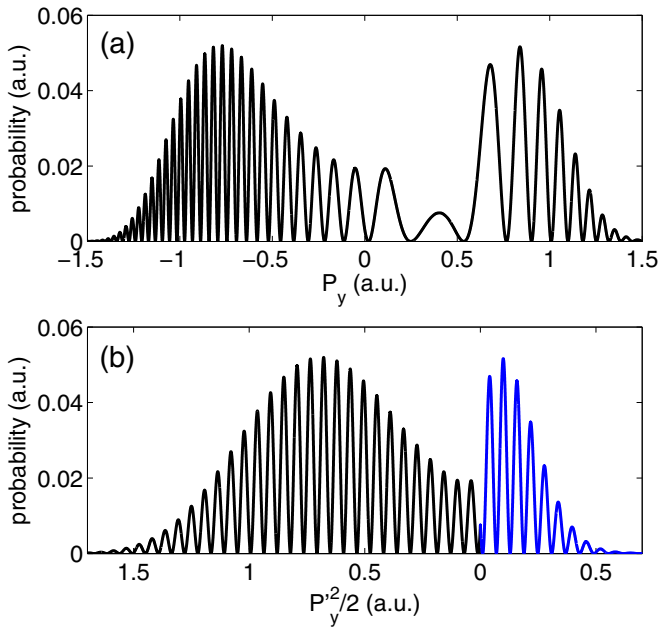

FIG. 2. (a) The photoelectron momentum at $p_x = 0$ in Fig. 1(f). (b) The kinetic energy spectrum $p_y'^2/2$, where $p_y' = p_y - 0.4$ a.u.. The black and blue parts correspond to $p_y' < 0$ and $p_y' > 0$.

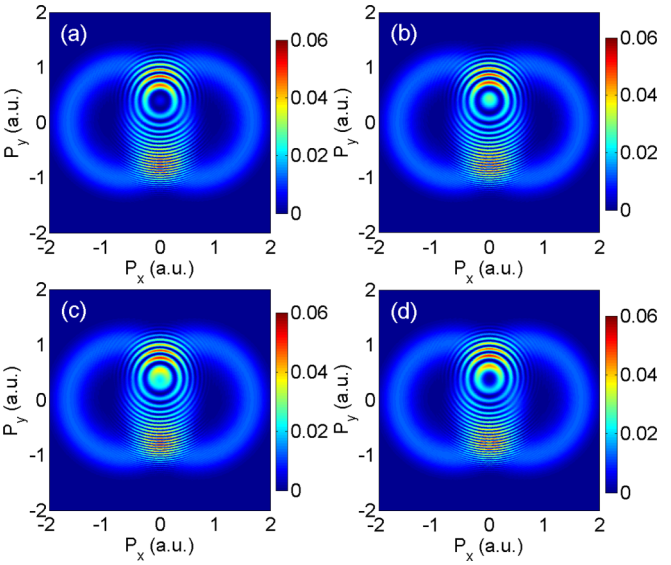

FIG. 3. PMDs when the CEP of the XUV2 is $\phi = 0$ (a), $\pi/2$ (b), π (c), and $3\pi/2$ (d). Other parameters are same as those used in Fig. 1(f).

have the phase difference

$$\begin{aligned}\Delta\phi^V &= S_p(t_2) - S_p(t_1) + I_p(t_2 - t_1) \\ &= \frac{T_{\rm mir}}{2}\frac{\boldsymbol{p}^2}{2} + \boldsymbol{p}\int_{t_1}^{t2} dt\boldsymbol{A}(t) + \frac{1}{2}\int_{t_1}^{t2} dt A^2(t) + \frac{T_{\rm mir}}{2} I_p \\ &= \frac{T_{\rm mir}}{2}\frac{(\boldsymbol{p} - \boldsymbol{p}_0)^2}{2} + C, \end{aligned} \tag{10}$$

where t_1 and t_2 are the timing when XUV1 and XUV2 appear, $\boldsymbol{p}_0 = \frac{-\int_{t_1}^{t'2} dt\boldsymbol{A}(t)}{T_{\rm mir}/2}$, and C is a constant by grouping other terms in Eq. (10) and not related to the electron final momentum. For the laser parameters used in Fig. 1(f), the calculated $p_{0,y} = \frac{-\int_{t_1}^{t'2} dt A_y(t)}{T_{\rm mir}/2} = 0.4$ a.u., which agrees with the numerical results exactly. The coefficient $T_{\rm mir}/2$ in Eq. (10) reflects for the energy separation $2\omega_{\rm mir}$ in Fig. 2(b). By the way, the momentum translation along the x axis in Figs. 1(e) and 1(f) is not governed by Eq. (10), but the term $\langle \mathbf{p} + \mathbf{A}(t)|$ in Eq. (1).

In the analysis of Eq. (10), the CEPs of the XUV pulses are not included. Simulations show that the fine structure in Fig. 1(f) is indeed affected by the XUV CEPs. Figure 3 shows the PMD when the CEP of XUV2 is (a) 0, (b) $\pi/2$, (c) π, and (d) $3\pi/2$. The maxima and minima along $p_x = 0$ sensitively depend on ϕ. However, the no-overlapped PMD initiated by two XUV pulses are ϕ independent. The ϕ-dependent concentric rings manifest themselves as Newton rings in classical optics. The PMD evolution with ϕ can be read from the Supplemental Material [44].

The ϕ dependence of the PMD at $p_x = 0$ can be used to retrieve the XUV CEP in experiment. As few-cycle XUV pulses have already been produced in laboratories [45], the calibration of the CEP of attosecond pulses may make it possible to visualize the sub-XUV-cycle dynamics. Figure 4 shows the density map of the p_y distribution as a function of ϕ, in which p_x is fixed at 0. The clear fluctuation around

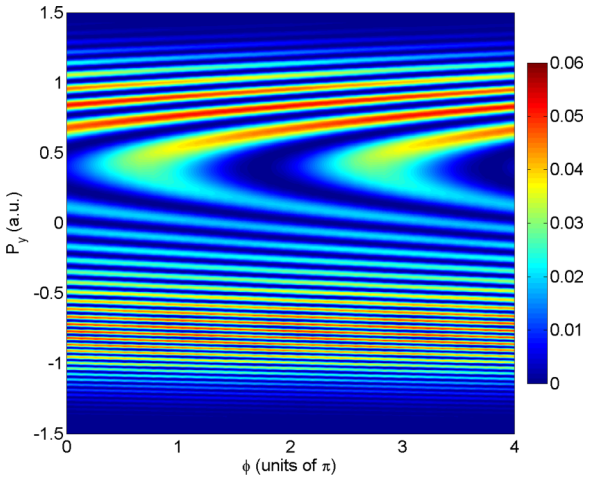

FIG. 4. The photoelectron momentum p_y at $p_x = 0$ as a function of ϕ. Other parameters are the same as those used in Fig. 1(f).

$p_y = 0.4$ a.u. makes perfect senses for ϕ measurement in current laser technologies.

In the above calculations, the MIR field is too weak to initiate comparable ionization with those initiated by XUV pulses. If MIR and XUV pulses contribute comparable ionization events, the PMD will show new structures. Figure 5(a) shows the PMD when the MIR and XUV intensities are 2×10^{14} W/cm^2 and 3×10^{13} W/cm^2. The ring with the center at $(p_x, p_y) = (0,0)$ and radius 2.05 a.u. is mainly contributed by the MIR field. The two small rings whose centers are at $(p_x, p_y) = (\pm 2.05, 0)$ are first produced by two XUV pulses and later streaked by the MIR field. As we stated above, the ionization events initiated by two XUV fields do not overlap and thus do not interfere with each other. However, in the areas where two small rings overlap with the big ring, interference appears. Further, in the arcs of the big ring that run through the two small rings, some maxima and minima occur. This angular distribution is produced by the overlapped XUV and MIR field. As explained in Ref. [46],

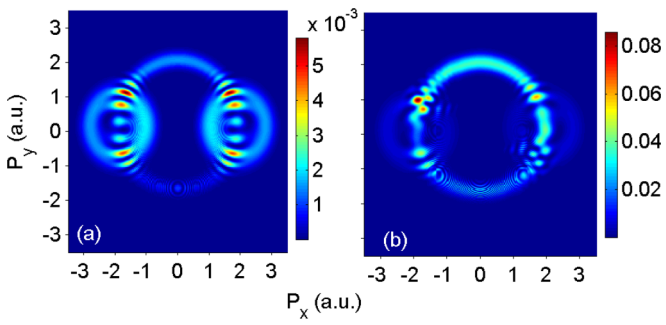

FIG. 5. The PMD induced by the combined circularly polarized XUV pulse train and circularly polarized MIR field based on the (a) SFA calculation and (b) time-dependent Schrödinger equation (TDSE) simulation. The XUV intensities are 3×10^{13} W/cm^2 and 3×10^{15} W/cm^2 in panels (a) and (b), respectively, and the MIR intensities are 2×10^{14} W/cm^2 for both panels. Other parameters are same as those used in Fig. 1(f).

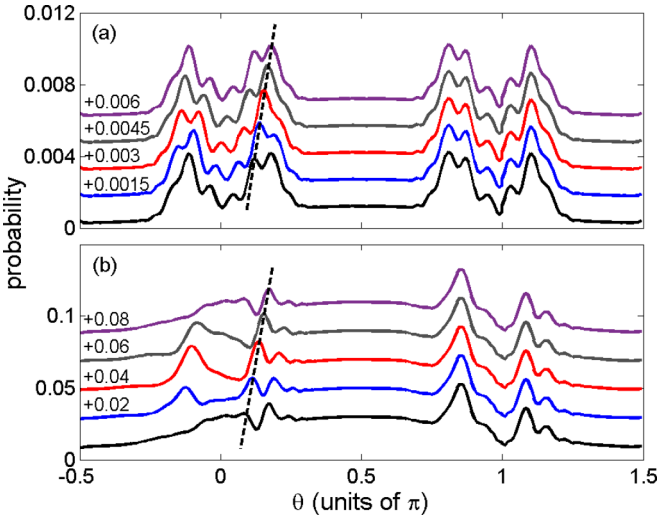

FIG. 6. The photoelectron angular distribution by radially integrating the MIR-induced tunneling photoelectron momentum distribution. Different curves correspond to $\phi = 0$, 0.5π, π, 1.5π, and 2π from bottom to up. These curves are vertically shifted for clear visualization. Other laser parameters are the same as those used in Fig. 5. The dashed lines mark the shift of the angular distribution.

the small fluctuated amplitude of the overlapped electric field is exponentially exaggerated into the tunneling ionization rate, and the local maximum ionization events are accelerated into different directions, thus forming the angular-resolved PMD.

Though SFA calculations may capture the main picture of photoionization, the neglected Coulomb potential will modify the PMDs. To justify the rationality of the above SFA calculations, we performed the numerical simulation of a two-dimensional TDSE, in which the electron movement is confined in the laser polarization plane. More details about the TDSE simulation can be found in Ref. [47]. The TDSE simulation result is shown in Fig. 5(b). Figures 5(a) and 5(b) share similar structures, which verifies that the SFA works for the given parameters.

The location of the angular maxima of the overlapped XUV and MIR field depends on the CEP of the XUV pulse. Thus, one may expect that the angular distribution of the PMD in the big ring also depends on the CEP of the XUV pulse. By radially integrating the PMD in the big rings, both generated by the SFA and TDSE calculations, we obtain the photoelectron angular distributions, as shown respectively in Figs. 6(a) and 6(b), in which different curves are corresponding to different CEPs and are vertically shifted for clear visualization. Other laser parameters are same as those used in Figs. 5(a) and 5(b). The fine structures around $\theta = \pi$ stay the same because the XUV1 pulse has a fixed CEP. In contrast, the distribution around $\theta = 0$ has the trend to move right with the increasing ϕ, as guided by the dashed lines in both panels of Fig. 6. Though the Coulomb potential modifies the details of the angular distribution, the XUV-CEP-dependent angular distribution is still observed. This angular-dependent PMD offers a perspective to retrieve the CEP of XUV pulses.

IV. CONCLUSIONS

In conclusion, our simulations show the PMD can be precisely tailored by the MIR and attosecond pulse train. By manipulating the MIR intensity, one can steer the two ionization events initiated by two XUV pulses in momentum representation, making them overlap or separate, and thus the interference pattern can be finely controlled. In the circular streaking, one component of the streaking field may only play a role in the Volkov phase instead of in the momentum shift for the final state. The CEP of the XUV pulse may change the fine structures of the PMD. The relative flat PMD in Fig. 5 can be used to extract the CEP of the XUV pulse. Alternatively, the CEP of the XUV pulse can also be retrieved by diagnosing the angular distribution of the PMD if the MIR field is strong enough to tunneling ionize the electron. Though ionization has been comprehensively studied, our study shows there are still a lot of intriguing phenomena about the ionization to be explored, and the ultrafast ionization process can be used to calibrate fundamental parameters, such as the CEP of XUV pulses.

ACKNOWLEDGMENTS

This work was supported by NSF of China (Grant No. 11322438, 11574205). Simulations were performed on the π supercomputer at Shanghai Jiao Tong University.

[1] T. Babrec and F. Krausz, Intense few-cycle laser fields: Frontiers of nonlinear optics, Rev. Mod. Phys. **72**, 545 (2000).

[2] D. J. Tannor, *Introduction to Quantum Mechanics: A Time-Dependent Perspective* (University Science Books, CA, Sausalito, 2007).

[3] E. Mevel, P. Breger, R. Trainham, G. Petite, P. Agostini, A. Migus, J. P. Chambaret, and A. Antonetti, Atoms in Strong Optical Fields: Evolution from Multiphoton to Tunnel Ionization, Phys. Rev. Lett. **70**, 406 (1993).

[4] W. Becker, F. Grasbon, R. Kopold, D. B. Milosevič, G. G. Paulus, and H. Walther, Above-threshold ionization: From classical features to quantum effects, Adv. At. Mol. Opt. Phys. **48**, 35 (2002).

[5] X. M. Tong, Z. X. Zhao, and C. D. Lin, Theory of molecular tunneling ionization, Phys. Rev. A **66**, 033402 (2002).

[6] M. Klaiber, K. Z. Hatsagortsyan, and C. H. Keitel, Tunneling Dynamics in Multiphoton Ionization and Attoclock Calibration, Phys. Rev. Lett. **114**, 083001 (2015).

[7] L. V. Keldysh, Ionization in the field of a strong electromagnetic wave, Sov. Phys. JETP **20**, 1307 (1965).

[8] J. L. Krause, K. J. Schafer, and K. C. Kulander, High-Order Harmonic Generation from Atoms and Ions in the High Intensity Regime, Phys. Rev. Lett. **68**, 3535 (1992).

[9] M. Lewenstein, Ph. Balcou, M. Yu. Ivanov, Anne L'Huillier, and P. B. Corkum, Theory of high-harmonic generation by low-frequency laser fields, Phys. Rev. A **49**, 2117 (1994).

[10] W. Becker, X. Liu, P. J. Ho, and J. H. Eberly, Theories of photoelectron correlation in laser-driven multiple atomic ionization, Rev. Mod. Phys. **84**, 1011 (2012).

[11] L. Zhang, X. Xie, S. Roither, Y. Zhou, P. Lu, D. Kartashov, M. Schöffler, D. Shafir, P. B. Corkum, A. Baltuška, A. Staudte, and M. Kitzler, Subcycle Control of Electron-Electron Correlation in Double Ionization, Phys. Rev. Lett. **112**, 193002 (2014).

[12] M. Richter, M. Kunitski, M. Schöffler, T. Jahnke, L. P. H. Schmidt, M. Li, Y. Liu, and R. Dörner, Streaking Temporal Double-Slit Interference by an Orthogonal Two-Color Laser Field, Phys. Rev. Lett. **114**, 143001 (2015).

[13] F. Mauger, A. Kamor, C. Chandre, and T. Uzer, Mechanism of Delayed Double Ionization in a Strong Laser Field, Phys. Rev. Lett. **108**, 063001 (2012).

[14] N. Dudovich, J. Levesque, O. Smirnova, D. Zeidler, D. Comtois, M. Yu. Ivanov, D. M. Villeneuve, and P. B. Corkum, Attosecond Temporal Gating with Elliptically Polarized Light, Phys. Rev. Lett. **97**, 253903 (2006).

[15] M. Li, L. Qin, C. Wu, L. Peng, Q. Gong, and Y. Liu, Rescattering and frustrated tunneling ionization of atoms in circularly polarized laser fields, Phys. Rev. A **89**, 013422 (2014).

[16] X. M. Tong, Z. X. Zhao, and C. D. Lin, Probing Molecular Dynamics at Attosecond Resolution with Femtosecond Laser Pulses, Phys. Rev. Lett. **91**, 233203 (2003).

[17] Z. Chen, A. T. Le, T. Morishita, and C. D. Lin, Origin of species dependence of high-energy plateau photoelectron spectra, J. Phys. B **42**, 061001 (2009).

[18] T. Morishita, A. T. Le, Z. Chen, and C. D. Lin, Accurate Retrieval of Structural Information from Laser-Induced Photoelectron and High-Order Harmonic Spectra by Few-Cycle Laser Pulses, Phys. Rev. Lett. **100**, 013903 (2008).

[19] J. Xu, Z. Chen, A. T. Le, and C. D. Lin, Self-imaging of molecules from diffraction spectra by laser-induced rescattering electrons, Phys. Rev. A **82**, 033403 (2010).

[20] C. I. Blaga, J. Xu, A. D. DiChiara, E. Sistrunk, K. Zhang, P. Agostini, T. A. Miller, L. F. DiMauro, and C. D. Lin, Imaging ultrafast molecular dynamics with laser-induced electron diffraction, Nature (London) **483**, 194 (2012).

[21] J. Xu, C. I. Blaga, P. Agostini, and L. F. DiMauro, Time-resolved molecular imaging, J. Phys. B **49**, 112001 (2016).

[22] M. Uiberacker, T. Uphues, M. Schultze, A. J. Verhoef, V. Yakovlev, M. F. Kling, J. Rauschenberger, N. M. Kabachnik, H. Schröder, M. Lezius, K. L. Kompa, H. G. Muller, M. J. J. Vrakking, S. Hendel, U. Kleineberg, U. Heinzmann, M. Drescher, and F. Krausz, Attosecond real-time observation of electron tunneling in atoms, Nature (London) **446**, 627 (2007).

[23] O. Kullie, Tunneling time in attosecond experiments, intrinsic-type of time: Keldysh and Mandelstam-Tamm time, J. Phys. B **49**, 095601 (2016).

[24] M. Chini, B. Zhao, H. Wang, Y. Cheng, S. X. Hu, and Z. Chang, Subcycle ac Stark Shift of Helium Excited States Probed with Isolated Attosecond Pulses, Phys. Rev. Lett. **109**, 073601 (2012).

[25] P. Ranitovic, X. M. Tong, C. W. Hogle, X. Zhou, Y. Liu, N. Toshima, M. M. Murnane, and H. C. Kapteyn, Controlling the XUV Transparency of Helium Using Two-Pathway Quantum Interference, Phys. Rev. Lett. **106**, 193008 (2011).

[26] F. He, C. Ruiz, A. Becker, and U. Thumm, Attosecond probing of instantaneous ac Stark shifts in helium atoms, J. Phys. B **44**, 211001 (2011).

[27] Y. Mairesse and F. Quéré, Frequency-resolved optical gating for complete reconstruction of attosecond bursts, Phys. Rev. A **71**, 011401(R) (2005).

[28] E. Goulielmakis, M. Uiberacker, R. Kienberger, A. Baltuska, V. S. Yakovlev, A. Scrinzi, Th. Westerwalbesloh, U. Kleineberg, U. Heinzmann, M. Drescher, and F. Krausz, Direct measurement of light waves, Science **305**, 1267 (2004).

[29] J. Gagnon, E. Goulielmakis, and V. S. Yakovlev, The accurate FROG characterization of attosecond pulses from streaking measurements, Appl. Phys. B **92**, 25 (2008).

[30] P. M. Paul, E. S. Toma, P. Breger, G. Mullot, F. Augé, Ph. Balcou, H. G. Muller, and P. Agostini, Observation of a train of attosecond pulses from high harmonic generation, Science **292**, 1689 (2001).

[31] P. Johnsson, J. Mauritsson, T. Remetter, A. L'Huillier, and K. J. Schafer, Attosecond Control of Ionization by Wave-Packet Interference, Phys. Rev. Lett. **99**, 233001 (2007).

[32] P. Ranitovic, X. M. Tong, B. Gramkow, S. De, B. DePaola, K. P. Singh, W. Cao, M. Magrakvelidze, D. Ray, I. Bocharova, H. Mashiko, A. Sandhu, E. Gagnon, M. M. Murnane, H. C. Kapteyn, I. Litvinyuk, and C. L. Cocke, IR-assisted ionization of helium by attosecond extreme ultraviolet radiation, New J. Phys. **12**, 013008 (2010).

[33] X. M. Tong, P. Ranitovic, C. L. Cocke, and N. Toshima, Mechanisms of infrared-laser-assisted atomic ionization by attosecond pulses, Phys. Rev. A **81**, 021404(R) (2010).

[34] F. Kelkensberg, W. Siu, J. F. Pérez-Torres, F. Morales, G. Gademann, A. Rouzée, P. Johnsson, M. Lucchini, F. Calegari, J. L. Sanz-Vicario, F. Martín, and M. J. J. Vrakking, Attosecond Control in Photoionization of Hydrogen Molecules, Phys. Rev. Lett. **107**, 043002 (2011).

[35] F. He and U. Thumm, Dissociative ionization of H_2 in an attosecond pulse train and delayed laser pulse, Phys. Rev. A **81**, 053413 (2010).

[36] E. S. Toma, H. G. Muller, P. M. Paul, P. Breger, M. Cheret, P. Agostini, C. Le Blanc, G. Mullot, and G. Cheriaux, Ponderomotive streaking of the ionization potential as a method for measuring pulse durations in the XUV domain with fs resolution, Phys. Rev. A **62**, 061801(R) (2000).

[37] E. Goulielmakis, V. S. Yakovlev, A. L. Cavalieri, M. Uiberacker, V. Pervak, A. Apolonski, R. Kienberger, U. Kleineberg, and F. Krausz, Attosecond control and measurement: Lightwave electronics, Science **317**, 769 (2007).

[38] M. Schultze, M. Fiess, N. Karpowicz, J. Gagnon, M. Korbman, M. Hofstetter, S. Neppl, A. L. Cavalieri, Y. Komninos, Th. Mercouris, C. A. Nicolaides, R. Pazourek, S. Nagele, J. Feist, J. Burgdörfer, A. M. Azzeer, R. Ernstorfer, R. Kienberger, U. Kleineberg, E. Goulielmakis, F. Krausz, and V. S. Yakovlev, Delay in photoemission, Science **328**, 1658 (2010).

[39] C. H. Zhang and U. Thumm, Streaking and Wigner time delays in photoemission from atoms and surfaces, Phys. Rev. A **84**, 033401 (2011).

[40] S. Cui and F. He, Time-resolved ionization process of hydrogen atoms in strong laser fields, Phys. Rev. A **88**, 063412 (2013).

[41] F. H. M. Faisal, Multiple absorption of laser photons by atoms, J. Phys. B **6**, L89 (1973).

[42] H. R. Reiss, Effect of an intense electromagnetic field on a weakly bound system, Phys. Rev. A **22**, 1786 (1980).

[43] D. B. Milošević and F. Ehlotzky, Scattering and reaction processes in powerful laser fields, Adv. At. Mol. Opt. Phys. **49**, 373 (2003).

[44] See Supplemental Material at http://link.aps.org/supplemental/10.1103/PhysRevA.94.053401 for the photoelectron momentum distribution evolves with the middle infrared laser intensity. Other parameters are same as those used in Figs. 1(e) and 1(f); the photoelectron momentum distribution evolves with the carrier envelope phase of the XUV2. Other parameters are same as those used in Fig. 3(a).

[45] G. Sansone, E. Benedetti, F. Calegari, C. Vozzi, L. Avaldi, R. Flammini, L. Poletto, P. Villoresi, C. Altucci, R. Velotta, S. Stagira, S. De Silvestri, and M. Nisoli, Isolated single-cycle attosecond pulses, Science **314**, 443 (2006).

[46] P. He, C. Ruiz, and F. He, Carrier-Envelope-Phase Characterization for an Isolated Attosecond Pulse by Angular Streaking, Phys. Rev. Lett. **116**, 203601 (2016).

[47] P. He and F. He, Ionization of H_2^+ in XUV pulses, Phys. Scr. **90**, 045402 (2015).